GOCI-Observed Chlorophyll Belts Associated With Sea-Surface Fronts in the East China Sea

Lei Chen, Changming Dong, and Guihua Wang

***Abstract*— Using chlorophyll-a observational data from the Geostationary Ocean Color Imager (GOCI) satellite operated by the Korean Satellite Center, thousands of high chlorophyll belts are found along the coast of East China Sea (ECS). These belts extend tens to hundreds of kilometers offshore with an average length of roughly 90 km and 18.3% occurrence probability. Through statistical analysis, appearance of these belts is characterized with a band oriented along the coastline direction around 100-km offshore with a maximum likely occurrence near 28.5°N. The instability of the coastal front plays an important role in the formation of the high-appearance band, and the eastward current associated with the estuarine front contributes to the maximum occurrence region around 28.5°N. These chlorophyll belts not only provide additional nutrients for phytoplankton growth but also are an important factor for the healthy coastal ecosystems.**

***Index Terms*— Chlorophyll, East China Sea (ECS), filament, front.**

I. Introduction

CHLOROPHYLL belts are long, thin horizontal chlorophyll filaments that form in the coastal ocean over a short period of time and are often associated with unstable ocean dynamic processes accompanied by ocean material advections. Chlorophyll belts have been frequently observed in the northeast Atlantic Ocean [1], off Cape Blanc, Mauritania [2], and in Monterey Bay, California [3]. The occurrence of these chlorophyll belts is primarily related to the presence of bioluminescent dinoflagellate species [4] and the impact of multiscale processes interacting with the local hydrography, the euphotic depth, and the nutrient distribution [5].

The ocean dynamics in the East China Sea (ECS) is greatly affected by the counterclockwise subtropical gyre circulation system comprised of the Kuroshio Current on the eastern side of the ECS, the Tsushima and Yellow Sea Warm Currents on the northern sides, and the coastal current on the western side [6]–[8]. For the eastern and northern sides, strong seasonal variations in surface chlorophyll concentration are presented [9]. For the western side, low salinity but high concentrations of nutrients and chlorophyll can be found [10]. A shift in maximum seasonal chlorophyll-a (Chl-a) concentration from July to September was observed between the mouth of the Changjiang River to an area east of Jeju Island [11]. The maximum Chl-a concentration represents an extension of the chlorophyll distribution that corresponds to the movement of Changjiang diluted water [12]. There have been few prior reports of chlorophyll belts south of Changjiang River mouth.

Some narrow Chl-a belts were found to the south of Changjiang River mouth in October and have been suggested to be associated with the cross-shelf jet, frontal instabilities, and multiple tongues of diluted water [13]. However, there are no systematic investigations of these belts. In this letter, we conduct a statistical analysis of the spatio-temporal characteristics of the chlorophyll belts south of the Changjiang River mouth (see Fig.1) and explore their potential formation mechanisms.

II. Data and Method

A. Data

Geostationary Ocean Color Imager (GOCI), operated by the Korean Satellite Center, is the first ocean color observation satellite to be placed in a geostationary orbit. The GOCI monitors marine environments along the northeast Asian coast in near real-time at a spatial resolution of 500 m. The GOCI observation platform allows for the hourly monitoring of variations in ocean properties like Chl-a from 9 A.M. to 16 P.M. (totally eight images) in a day [14]. GOCI has six visible bands centered at 412, 443, 490, 555, 660, and 680 nm, and two near-infrared bands centered at 745 and 865 nm [15]. The Chl-a data (https://oceandata.sci.gsfc.nasa.gov/GOCI/L2/) employed in this letter is the daily average product from April 1, 2011 to December 31, 2017.

The sea surface temperature (SST) data taken from the Remote Sensing System (ftp://data. remss.com/SST/

Manuscript received June 2, 2019; revised September 3, 2019; accepted October 4, 2019. Date of publication October 25, 2019; date of current version July 22, 2020. The work of C. Dong was supported in part by the National Key Research and Development Program of China under Grant 2017YFA0604100 and Grant 2016YFA0601803, in part by the National Natural Science Foundation of China under Grant 41476022 and Grant 41490643, in part by the Startup Foundation for Introducing Talent of Nanjing University of Information Science and Technology under Grant 2014r072, in part by the Program for Innovation Research and Entrepreneurship team in Jiangsu Province under Grant 2191061503801, in part by the National Programme on Global Change and Air-Sea Interaction under Grant GASI-03-IPOVAI-05, and in part by the foundation of China Ocean Mineral Resources Research and Development Association under Grant DY135-E2-2-02 and Grant DY135-E2-3-01. The work of G. Wang was supported in part by the National Natural Science Foundation of China under Grant 41976003 and Grant 41576002, in part by the Program of Shanghai Academic/Technology Research Leader under Grant 17XD1400600, and in part by the National Key Research and Development Program of China under Grant 2017YFC1404103. *(Corresponding author: Guihua Wang.)*

L. Chen is with the School of Marine Sciences, Nanjing University of Information Science and Technology, Nanjing 210094, China.

C. Dong is with the Southern Laboratory of Ocean Science and Engineering, School of Marine Sciences, Nanjing University of Information Science and Technology, Nanjing 210094, China.

G. Wang is with the Department of Atmosphere and Ocean Sciences, Institute of Atmospheric Sciences, CMA-FDU Joint Laboratory of Marine Meteorology, Fudan Univerisity, Shanghai 200433, China (e-mail: wghocean@yahoo.com).

Color versions of one or more of the figures in this letter are available online at http://ieeexplore.ieee.org.

Digital Object Identifier 10.1109/LGRS.2019.2947175

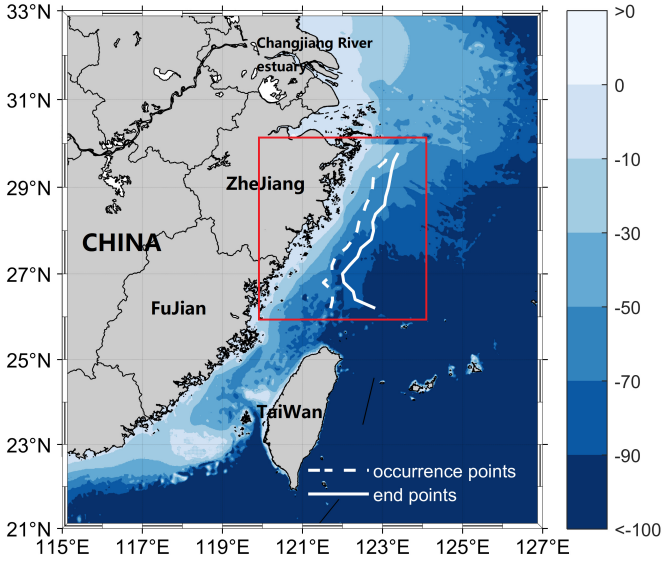

Fig. 1. ECSs bathymetry (m). The red box delineates the study area (120°E–124°E, 26°N–30°N). The dashed (solid line) white line is the average occurrence (end) points of high chlorophyll belts for each 0.2 meridional grids.

daily _v04.0/mw_ir/) has a spatial resolution of 9 km × 9 km and a temporal sampling frequency of 1 day. The SST data set is combined with infrared measurements from the Moderate Resolution Imaging Spectroradiometer, and microwave measurements from the Advanced Earth Observation System's Microwave Scanning Radiometer, the Tropical Rainfall Measurement Mission and the WindSAT. All of these data products cover the time period from 2011 to 2017.

B. Chlorophyll-a Belt Detection

The method used to identify the Chl-a belts consists of two steps: First, in order to outline high Chl-a concentration regions, high chlorophyll value areas are marked in each image. It should be noted that the values higher than the surroundings are selected and the middle points of the high Chl-a concentration at each longitude are identified. Second, using the identification of the points within a belt, the chlorophyll concentration is interpolated from the longitude and latitude of the marked points, so as to obtain the instantaneous position and intensity of the chlorophyll belt. Only those belts originating from the western coast of the ECS are considered in this letter.

III. Results

A. Observation of the Chlorophyll Belts

Using data from the high-resolution ocean color remote sensing GOCI satellite, we found a set of fascinating beard-like chlorophyll belts off the western coast of the ECS. These belts possess a great deal of complexity and fine scale structure. A snapshot of Chl-a on August 10, 2011 [see Fig. 2(a)] shows two Chlorophyll belts: one starts at around 27.8°N, 121.5°E and extends northeastward to 28.8°N, 123.5°E, and the other occurs at around 27.2°N, 121°E and runs roughly parallel to the first belt, extending 250-km offshore. Three

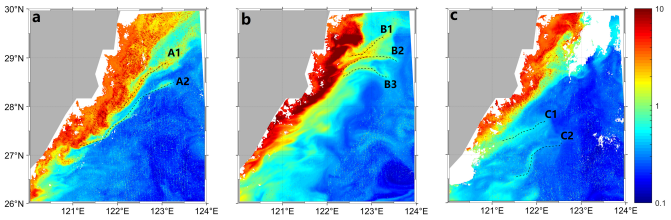

Fig. 2. Snapshots of GOCI sea surface Chl-a concentration (shaded, mgm^{-3}) on (a) August 10, 2011, (b) August 3, 2013, and (c) July 28, 2011. The Chl-a belts (labeled A1, A2, B1, B2, B3, C1, and C2) are indicated by the dashed lines.

shorter chlorophyll belts were also observed north of 27.5°N on August 3, 2013 [see Fig. 2(b)] and two weaker chlorophyll belts which formed south of 27°N were identified on July 28, 2011 [see Fig. 2(c)]. These snapshots demonstrate that the Chl-a belts can develop anywhere in the letter area. To understand the general characteristics of Chl-a belts, Fig. 3(a) shows the distribution of all the Chl-a belts identified from the daily GOCI images between April 2011 and December 2017. In the nearly seven years, chlorophyll belts were observed for 451 days, accounting for 18.3% of the total number of days. In total, 1888 belts were identified between 26°N and 30°N over the entire time period.

Table I lists the occurrence date, occurrence frequency, number, length, and concentration of the chlorophyll belts observed for each year of the study period. The results show that there is significant interannual variation in the timing and frequency of the belts. On average, the belts are about 90 km in length and have a Chl-a concentration of about 0.06 mgm^{-3}. Overall, chlorophyll belts are present between 12.05% and 23.29% of the time. The probability (P_1) is calculated by dividing the number of days that chlorophyll bands appear by the total days for that year. The number and days of chlorophyll belts that appeared in the selected area was exceptionally high in 2013 and 2016, while in the remaining years they were less frequent. However, we should note that the chlorophyll data from the GOCI satellite record began in April of 2011, which partly explains the low number of belts that year. In addition, the observation of Chl-a is highly affected by cloud cover, which can also have impacts on the belt occurrence frequency. The probability (P_2), the number of days with the bands divided by the total number of days only with few cloud cover (less than 5% cloud cover used here), is also listed in Table I.

The distribution of chlorophyll belts shows a relatively dense band in the region around 26.5°N and 29.5°N [see Fig. 3(b)]. This band extends along a southwest to the northeast oriented axis that is nearly parallel to the 50 to 100 m isobaths [see Fig. 3(c)]. If 70 belts are applied as the minimum to define the band area, then the western side of the band is about 50 km off the coast at around 27°N, and it moves offshore as it extends northward. In addition, the bandwidth is about 30 km in the south to 100 km in the north with an average width of 50 km.

Although the number of chlorophyll belts varied from month to month, they appeared most frequently from July to September every year and are relatively absent in other

TABLE I

STATISTICS OF THE CHLOROPHYLL BELTS IDENTIFIED IN THE DAILY GOCI CHLOROPHYLL-A IMAGES OF THE ECS BETWEEN 2011 AND 2017

Year	2011	2012	2013	2014	2015	2016	2017
No.	142	168	435	284	240	357	262
Days	38	44	83	60	54	85	74
P_1	13.81%	12.05%	22.74%	16.38%	14.79%	23.29%	20.27%
P_2	20.77%	21.78%	38.07%	25.32%	24.22%	37.12%	32.03%
T_{first}	04-20	05-05	01-21	01-01	01-14	03-03	02-13
T_{last}	11-01	11-19	12-03	12-17	11-23	11-16	10-04
<L>	87.782	89.037	91.413	86.791	102.48	102.67	91.383
Max(L)	277.57	200.48	216.20	206.58	238.14	269.42	200.55
Min(L)	21.393	29.312	23.529	28.696	30.877	27.765	28.458
<S>	1.3076	1.6197	1.4787	1.6622	1.7932	1.5563	1.4284
Max(S)	6.2499	9.4121	9.1680	10.447	16.838	10.991	13.394
Min(S)	0.2861	0.2483	0.2472	0.2429	0.2651	0.2093	0.2369

Note: No.: number of Chlorophyll belts; Days: the total number of days that chlorophyll bands appear in the year; P_1: occurrence probability; P_2:Cloud cover removed occurrence probability; T_{first}: date of the first appearance of belts; T_{last}: date of the disappearance of belts; L: length of the belt (defined as the curvilinear distance between a belt's initial and final positions, in km); S: Chlorophyll concentration within the belts (in mg·m^{-3}); < >: average of the group.

months. While part of the reason for their absence between October and June may be due to missing satellite observation as a result of cloud cover, the low survival rate of phytoplankton in winter reduces the chlorophyll levels so that belts are difficult to observe. The similarity between July–September results [see Fig. 3(b)] and those for the entire year [see Fig. 3(c)] suggests that July–September are the dominant months for the number of chlorophyll belts.

Looking at the spatial extent of the area with relatively dense chlorophyll belts from July to September, the region has a similar pattern but with large spatial variability [see Fig. 3(d)]. In all the three months, the band is aligned in a southwest to northeast direction along the 50-m isobath and has a maximum that occurs around 28.5°N. However, from July to September, the area becomes smaller and narrower, with a decrease in area from 30 000 km in July to about 5000 km by September [see Fig. 3(d)].

B. Formation Mechanism for High Chlorophyll Belt Occurrence Zone

To understand the above discussed factors for the existence of these dense bands and the central regions, we use the high-resolution daily sampled SST data during the summer period from July to September for all years to identify the coastal front. By comparison, it is apparent that the chlorophyll bands are nearly parallel to the isotherms [see Fig. 4(a)].

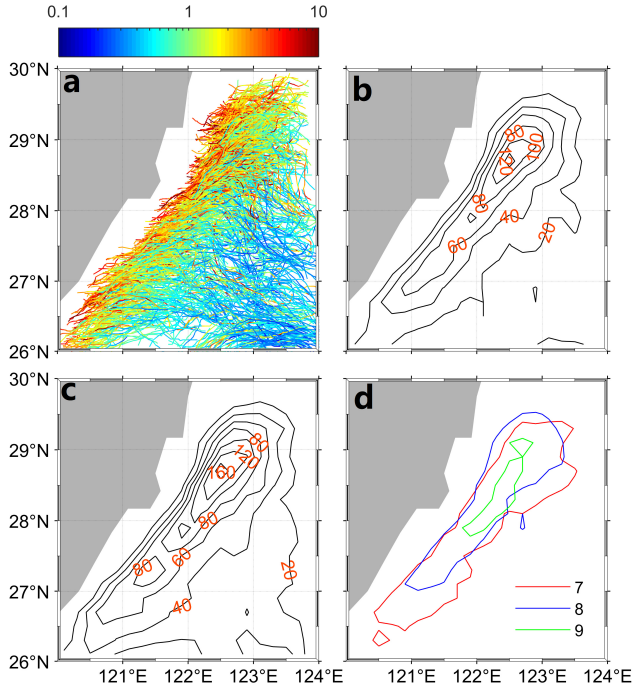

Fig. 3. (a) Distribution of all the chlorophyll belts identified in the daily GOCI Chlorophyll-a images of the eastern ECS during 2011–2017. The colorbar represents chlorophyll concentration within the belts (in mg·m^{-3}). (b) Chlorophyll belts in each 0.2 × 0.2 box in the eastern ECS from July to September of 2011–2017. (c) Chlorophyll belts in each 0.2 × 0.2 box in the eastern ECS for all months of 2011–2017. (d) Spatial extent of the maximum bands from July to September over the 2011–2017 time period.

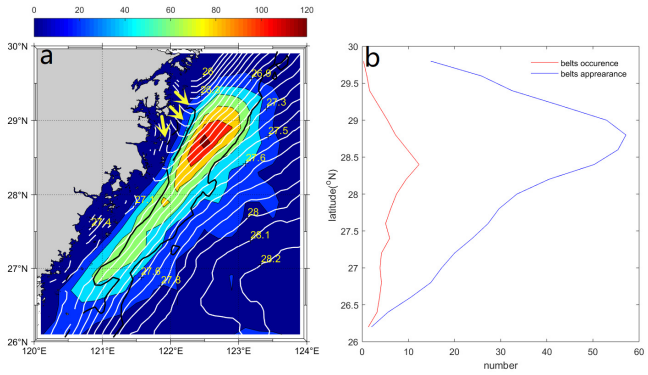

Fig. 4. (a) Composites of the SST (white contours at 0.1 °C intervals), estuarine terrain, eastward current (yellow arrow), coastal front (black contour of SST gradient at 0.4°/100 km), and chlorophyll belts from July to September of 2011–2017 (shading). The colorbar represents the number of chlorophyll belts. (b) The average number of belts at each 0.2° latitude for belts appearance (blue line) and belts occurrence (red line).

The sharp lateral gradient larger than 0.4°/100 km in the isotherms is applied to represent the coastal front, whose area is roughly surrounded by the black contour in Fig. 4(a). The Zhejiang–Fujian coastal front (along the 50-m isobath) on the western boundary of the ECS has an average length of 740 km in summer (see Fig. 4(a) and [16]). It is valuable to know that the location of this coastal front is almost the same as that of the high Chl-a appearance band [see Fig. 4(a)], suggesting that the coastal front may play an important role of the high Chl-a appearance band. The possible dynamic linkages

between them can follow as below. Most coastal fronts are intrinsically unstable. It is thus highly favored to generate cross-shelf penetrating currents off the coast. These cross-shelf penetrating currents may carry high, nearshore chlorophyll into the interior of the ECS, to form a chlorophyll belt. These dynamic processes are quite similar to those suggested by Yuan *et al*. [13], which indicated that currents associated with coastal frontal instability can transport waters with high chlorophyll concentrations offshore in the South of Changjiang river mouth. Therefore, we surmise that the instability of the long coastal front extending southwest to northeast along the Zhejiang–Fujian coast can explain the spatial patterns of the high chlorophyll bands.

Fig. 4(b) shows the zonal average of chlorophyll belt appearance and the chlorophyll belt occurrences. The nearest offshore location of the chlorophyll belt is defined as the original point of the chlorophyll belt. When the original point occurs in one grid, the belt occurrence is counted at the grid point once. For the belt appearance, each time when the belt passes through a grid point, it is counted once for the belt appearance in the grid point. We found that chlorophyll belt appearance and the chlorophyll belt occurrences are quite similar; both showing a maximum around 28.5°N, suggesting that there is a mechanism that triggers the occurrence of a high chlorophyll belt. As shown in Fig. 4(a), the isotherms between 28.5°N and 29.5°N near the coast are tongue-shaped, which suggests an eastward current exists in this region [yellow vector shown in Fig. 4(a)]. We propose the following dynamical process: cold, chlorophyll-rich water from Changjiang and Qiantang rivers accumulates in the near-shore region north of 28.5°N. South of this cold water pool, an eastward current associated with the estuarine front develops through a strong density gradient. This eastward current then transports the near-shore, high chlorophyll water to offshore region, which feeds the maximum occurrence region of high chlorophyll.

IV. Conclusion

The spatial distribution and its temporal variation of chlorophyll belts along the Zhejiang–Fujian coast in the ECS are analyzed. These chlorophyll belts, which often form along the 50–100-m isobath of the ECS and extend hundreds of kilometers offshore, are the manifestation of frontal instability currents that transport nutrient-rich, high-chlorophyll water from the coastal zone into the interior of the ECS. The average occurrence point of the chlorophyll belt and the endpoint of the chlorophyll belts [see Fig. 1] indicate that Chlorophyll can be transported roughly 90-km offshore.

The appearance of these chlorophyll belts demonstrates a high concentration around 100-km offshore oriented in a southwest to northeast direction and can be attributed to the coastal front whose instability can trigger significant cross-shelf jets [13]. Furthermore, the maximum occurrence region (around 28.5°N) of these chlorophyll bands is likely due to the precise location of the eastward current associated with the estuarine front. However, in order to verify and elucidate the dynamic mechanisms of these bands, simulations using a high-resolution coupled numerical circulation model containing advanced mixed layer physics are required.

These chlorophyll belts, also known as coastal phytoplankton filaments [17], migrate away from the coast and thereby provide additional nutrient resources for phytoplankton growth within the ECS. Thus, the chlorophyll belts may be an important factor affecting the health of coastal ecosystems. For example, these nutrient transports may result in harmful algae blooms (HABs) during the healthy ecosystem development [3]. All of these emphasize the importance of further observation and simulation to understand these development processes of the chlorophyll belt.

References

[1] Y. Lehahn, F. D'Ovidio, M. Levy, and E. Heifetz, "Stirring of the northeast Atlantic spring bloom: A Lagrangian analysis based on multisatellite data," *J. Geophys. Res., Oceans*, vol. 112, no. C8, Aug. 2007, Art. no. C08005.

[2] L. Van Camp, L. Nykjaer, E. Mittelstaedt, and P. Schlittenhardt, "Upwelling and boundary circulation off Northwest Africa as depicted by infrared and visible satellite observations," *Prog. Oceanogr.*, vol. 26, no. 4, pp. 357-402,1991.

[3] I. Shulman, B. Penta, J. Richman, G. Jacobs, and S. Anderson, "Impact of submesoscale processes on dynamics of phytoplankton filaments," *J. Geophys. Res., Oceans*, vol. 120, no. 3, pp. 2050–2062, Mar. 2015.

[4] M. A. Moline *et al.*, "Bioluminescence to reveal structure and interaction of coastal planktonic communities," *Deep Sea Res. II, Top. Stud. Oceanogr.*, vol. 56, nos. 3–5, pp. 232–245, Feb. 2009.

[5] M. Lévy, R. Ferrari, P. J. S. Franks, A. P. Martin, and P. Rivière, "Bringing physics to life at the submesoscale," *Geophys. Res. Lett.*, vol. 39, no. 14, Jun. 2012, Art. no. L14602.

[6] B.-X. Guan, "Patterns and structures of the currents in Bohai, Huanghai and East China Seas," *Oceanol. China Seas*, to be published.

[7] H. Ichikawa and R. C. Beardsley, "The current system in the Yellow and East China Seas," *J. Oceanogr.*, vol. 58, no. 1, pp. 77–92, 2012.

[8] C.-T. A. Chen, "Chemical and physical fronts in the Bohai, Yellow and East China seas," *J. Mar. Syst.*, vol. 78, no. 3, pp. 394–410, 2009.

[9] L. Yu, X.-H. Zhu, X. Guo, and H. Huang, "Temporal variation of Kuroshio nutrient stream south of Japan," *J. Geophys. Res., Oceans*, vol. 123, no. 11, pp. 7896–7913, Nov. 2018.

[10] X. Ning, Z. Liu, Y. Cai, F. Chai, and M. Fang, "Physicobiological oceanographic remote sensing of the East China Sea: Satellite and in situ observations," *J. Geophys. Res., Oceans*, vol. 103, no. C10, pp. 21623–21635, Sep. 1998.

[11] H. Yamaguchi, J. Ishizaka, E. Siswanto, Y. B. Son, Y. Sinjae, and Y. Kiyomoto, "Seasonal and spring interannual variations in satellite-observed chlorophyll-a in the Yellow and East China Seas: New datasets with reduced interference from high concentration of resuspended sediment," *Continental Shelf Res.*, vol. 59, pp. 1–9, May 2013.

[12] H. Yamaguchi *et al.*, "Seasonal and summer interannual variations of SeaWiFS chlorophyll a in the Yellow Sea and East China Sea," *Prog. Oceanogr.*, vol. 105, pp. 22–29, Oct. 2012.

[13] D. Yuan, F. Qiao, and J. Su, "Cross-shelf penetrating fronts off the southeast coast of China observed by MODIS," *Geophys. Res. Lett.*, vol. 32, no. 19, 2015, Art. no. L19603.

[14] J.-K. Choi, Y. J. Park, J. H. Ahn, H.-S. Lim, J. Eom, and J.-H. Ryu, "GOCI, the world's first geostationary ocean color observation satellite, for the monitoring of temporal variability in coastal water turbidity," *J. Geophys. Res., Oceans*, vol.117, no. C9, 2012, Art. no. C09004.

[15] J.-K. Choi, Y. J. Park, B. R. Lee, J. Eom, J.-E. Moon, and J.-H. Ryu, "Application of the Geostationary Ocean Color Imager (GOCI) to mapping the temporal dynamics of coastal water turbidity," *Remote Sens. Environ.*, vol. 146, pp. 24–35, Apr. 2014.

[16] W. Huang, X. Lou, J. Yang, A. Shi, Q. Xiao, and C. Lin, "Satellite observation of the Zhejiang-Fujian coastal front in the East China Sea," in *Proc. IEEE Int. Geosci. Remote Sens. Symp.*, Sep. 2004, pp. 3489–3491.

[17] E. R. Abraham, C. S. Law, P. W. Boyd, S. J. Lavender, M. T. Maldonado, and A. R. Bowie, "Importance of stirring in the development of an iron-fertilized phytoplankton bloom," *Nature*, vol. 407, pp. 727–730, Sep. 2000.